

PREPARED FOR SUBMISSION TO JHEP

Long-lived particle phenomenology in one-loop neutrino mass models with dark matter

Carolina Arbeláez,^a Giovanna Cottin,^{b,c} Juan Carlos Helo,^{d,e} Martin Hirsch,^e Téo B. de Melo^{c,f,g}

^a*Universidad Técnica Federico Santa María and Centro Científico Tecnológico de Valparaíso CCTVal, Casilla 110-V, Valparaíso, Chile*

^b*Instituto de Física, Pontificia Universidad Católica de Chile, Avenida Vicuña Mackenna 4860, Santiago, Chile*

^c*Millennium Institute for Subatomic Physics at the High Energy Frontier (SAPHIR), Fernández Concha 700, Santiago, Chile*

^d*Departamento de Física, Facultad de Ciencias, Universidad de La Serena, Avenida Cisternas 1200, La Serena, Chile*

^e*Instituto de Física Corpuscular (CSIC-Universitat de València), C/ Catedrático José Beltrán 2, E-46980 Paterna (València), Spain*

^f*Universidad Andrés Bello, Facultad de Ciencias Exactas, Departamento de Ciencias Físicas-Center for Theoretical and Experimental Particle Physics, Fernández Concha 700, Santiago, Chile*

^g*Universidad Viña del Mar, Escuela de Ciencias, Agua Santa 7055, Rodelillo, Viña del Mar, Chile*
E-mail: carolina.arbelaez@usm.cl, gfcottin@uc.cl, jchelo@userena.cl, mahirsch@ific.uv.es, tessio.melo@uvm.cl

ABSTRACT:

Neutrino masses and dark matter (DM) might have a common origin. The *scotogenic* model can be considered the proto-type model realizing this idea, but many other variants exist. In this paper we explore the phenomenology of a particular DM neutrino mass model, containing a triplet scalar. We calculate the relic density and check for constraints from direct detection experiments. The parameter space of the model, allowed by these constraints, contains typically a long-lived or quasi-stable doubly charged scalar, that can be searched for at the LHC. We reinterpret existing searches to derive limits on the masses of the scalars of the model and estimate future sensitivities in the high-luminosity phase of the LHC. The searches we discuss can serve to constrain also many other 1-loop neutrino mass models.

Contents

1	Introduction	1
2	Setup: Model and implementation	3
2.1	Model lagrangian and mass matrices	3
2.2	Model implementation and decay widths	6
3	Dark matter phenomenology	8
4	Collider phenomenology	11
5	Summary and discussion	15

Contents

1 Introduction

The main idea of the famous scotogenic model [1, 2] is that neutrino masses and dark matter (DM) might share a common origin. The model is rather simple: It adds a second Higgs doublet, η , and three right-handed neutrinos, N_i , to the SM particle content. In addition, these new fields are assumed to be odd under a discrete Z_2 symmetry.¹ The lightest Z_2 odd particle, either N_1 or the lightest neutral component in η , can be a good DM candidate, while neutrino masses are generated via a 1-loop diagram, see fig. 1, left.

The phenomenology of the scotogenic model has been studied in many papers. For the case of η^0 being the lightest Z_2 -odd particle, the DM phenomenology of the scotogenic model resembles closely the inert doublet model [3]. Fermionic DM and lepton flavour violation bounds on model parameters have been calculated in [4]. A very light N_1 in the scotogenic model could be a FIMP (“feebly interacting massive particle”), see for example [5–7]. Indirect detection of the DM in the scotogenic model was discussed in [8, 9]. The collider phenomenology for the case of a real scalar dark matter candidate was discussed in [10, 11]. For the expectations for the scotogenic model at a future muon collider see [12].

A number of variations of the scotogenic model have also been discussed. Examples are the “scoto-singlet” model (adding a $S_{1,1,0}$)² [13] or the type-I/III variant (adding a fermionic triplet, $F_{1,3,0}$) [14]. A version with two inert doublet scalars (and only one N) was presented in [15]. A generalization of the scotogenic model to an arbitrary number of

¹The new scalar has also to be inert, i.e. $\langle\eta^0\rangle = 0$, which is easy to arrange.

²We will use S (F) for a scalar (fermion) BSM field, with the subscripts denote the properties of the field under the SM gauge group $SU(3)_C \times SU(2)_L \times U(1)_Y$.

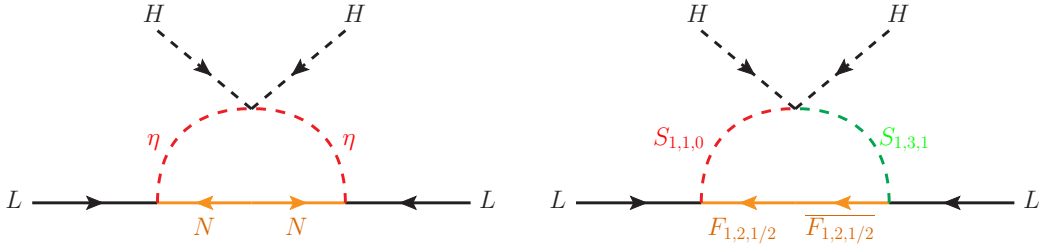


Figure 1. The Weinberg operator generated at 1-loop level in two example dark matter models. To the left: The original scotogenic model ($\eta = S_{1,2,1/2}$, $N = F_{1,1,0}$), to the right the singlet-triplet model that we will study in detail in this work.

generations (both scalars and fermions) was discussed in [16]. Adding a Z' to the model allows to motivate the Z_2 (which is put by hand in the original model) and affects drastically the relic density of the N in the scotogenic model, as discussed in [17]. A general list of UV extensions that could explain the Z_2 of the scotogenic model was given in [18]. Spontaneous breaking of lepton number in a scotogenic setup was considered in [19]. All these variations keep η and N_i as the basic ingredient of the models. However, there is also [20], which uses two scalar triplets instead of η and [21] with a scalar triplet and a scalar singlet.

On the other hand, there are many possible 1-loop neutrino mass models. A general classification of genuine 1-loop neutrino mass diagrams can be found in [22]. A list of possible, phenomenologically consistent realizations has been given in [23]: There are in principle two classes of models. First, there are models in which the lightest loop particle is either a SM field or can decay to some SM fields; these are called “exit” models in [23]. The second class contains some BSM multiplet whose lightest member is electrically neutral and thus can be a good cold dark matter candidate. The list of such DM models in [23] is restricted to multiplets with hypercharge at most $Y = 1$, such that stringent constraints from direct detection experiments can be avoided [24, 25]. With this condition [23] counts a total 318 of DM models.

One can consider the scotogenic model as the *proto-type* model for the DM model class. However, all of the DM models can explain the observed [26] relic density of dark matter, obey bounds from direct detection (DD) experiments [27, 28], fit neutrino oscillation data [29] and fulfill limits from charged lepton flavour violation searches [4, 30]. Thus, it seems, collider observables are the only possible way to distinguish between (at least some of the) DM model variants. ³

One particular example model from [23] is shown in fig. 1, right. We will call this the scalar singlet-triplet (SST) model below. Clearly, the presence of the scalar triplet, $S_{1,3,1}$, will give rise to signals potentially very different from the scotogenic model. The aim of

³A disclaimer is needed here. If a signal in direct detection experiment were found, the mass of the WIMP, m_{DM} could be determined, if m_{DM} is small. However, for WIMP masses larger than the target nucleus mass, the recoil spectrum becomes nearly independent of m_{DM} and only a lower limit on m_{DM} can be given in this case [31, 32].

our present work is to study the LHC phenomenology of the SST model in some detail. As discussed in section 5, the signals we consider in this paper will appear in many other models in the list of models from [23], too.

The rest of this paper is organized as follows. In section 2 we present the model variant, that we will study in detail. Then, in section 3 we discuss briefly dark matter phenomenology of the model. This study allows us to identify parameter regions, where the model gives the correct relic density and obeys the current bound from DD experiments. With hindsight, we calculate the decay lengths ($c\tau$) of the doubly charged member of the scalar triplet, t^{++} , and find that (i) the relic density calculation favours points with moderate to small mass splitting between the scalar singlet and triplets and (ii) in this mass region parameter points that pass *future* direct detection bounds have usually tiny decay widths for the t^{++} . Section 4 then forms the main body of this work. Different possible searches for t^{++} at the LHC are discussed, current and future sensitivities are estimated.

Finally, in section 5 we summarize the current paper and give also a qualitative discussion, how our results can be applied to other 1-loop DM model variants listed in [23]. Given the large number of possible models, this discussion necessarily has to be rather superficial, but it serves to list possible signals that would allow to distinguish many models from the proto-type scotogenic model.

2 Setup: Model and implementation

2.1 Model lagrangian and mass matrices

The model we study in detail in this paper introduces two new scalars and three vector-like fermions. The quantum numbers of all new fields are given in table 1.

Fields	$SU(3)_C$	$SU(2)_L$	$U(1)_Y$	\mathbb{Z}_2
(Real) S_1	1	1	0	–
S_3	1	3	1	–
F (\bar{F})	1	2	1/2 (–1/2)	–

Table 1. Quantum numbers for the particle content of the model. While neutrino masses could be explained already with one copy of F/\bar{F} , in our numerical study we use three families of F/\bar{F} to reflect the number of generations in the SM.

The triplet scalar can be written in the usual way:

$$S_3 = \begin{pmatrix} t^+/\sqrt{2} & t^{++} \\ t^0 & -t^+/\sqrt{2} \end{pmatrix}. \quad (2.1)$$

The Lagrangian of the model adds the following terms to the SM Lagrangian:

$$\begin{aligned} \mathcal{L} = & - (M_F F \bar{F} + M_{S_1}^2 |S_1|^2 + M_{S_3}^2 |S_3|^2) - (h_F L F S_1 + h_{\bar{F}} L \bar{F} S_3 + \text{h.c.}) \\ & + \lambda_2 |H|^2 |S_1|^2 + \left(\lambda_{3a} |H|^2 |S_3|^2 + \lambda_{3b} \epsilon_{l_1 l_3} \epsilon_{l_2 l_4} \epsilon_{l_{3b} l_{4b}} H_{l_1} H_{l_2}^* (S_3)_{l_3 l_{3b}} (S_3^*)_{l_4 l_{4b}} \right) \end{aligned} \quad (2.2)$$

$$\begin{aligned}
& + \lambda_4(|S_1|)^4 - (\lambda_5 H H S_1 S_3^\dagger + \text{h.c}) \\
& + \left(\lambda_{6a}(|S_3|)^4 + \lambda_{6b} \epsilon_{l_1 l_3} \epsilon_{l_{1b} l_{3b}} \epsilon_{l_2 l_4} \epsilon_{l_{2b} l_{4b}} (S_3)_{l_1 l_{1b}} (S_3^*)_{l_2 l_{2b}} (S_3)_{l_3 l_{3b}} (S_3^*)_{l_4 l_{4b}} \right) + \lambda_7 |S_1|^2 |S_3|^2.
\end{aligned}$$

The terms proportional to λ_3 and λ_6 have two independent $SU(2)_L$ contractions each. We calculated these and cross-checked for consistency with **Sym2Int** [33]. The couplings λ_{6a} , λ_{6b} and λ_7 describe only scatterings among the BSM scalars S_1 and S_3 , for collider and dark matter phenomenology they are mostly irrelevant and will therefore not be discussed in detail in the rest of this paper. M_F , in general, is a 3×3 matrix. We can always choose a basis, such that M_F is diagonal and real, with eigenvalues m_{F_i} . The Yukawa matrices h_F , $h_{\bar{F}}$ are 3×3 non-diagonal and can be complex in general. From the quartic couplings, the most important one is λ_5 . In the limit $\lambda_5 \rightarrow 0$, the model conserves lepton number and neutrino masses are zero.

After electroweak symmetry breaking the neutral part of the scalars in S_1 and S_3 mix. Their (tree-level) mass matrix is given by:

$$M_S^0 = \begin{pmatrix} M_{S_3}^2 - \frac{\lambda_{3a} v^2}{2} & \frac{\lambda_5 v^2}{\sqrt{2}} \\ \frac{\lambda_5 v^2}{\sqrt{2}} & M_{S_1}^2 - \frac{\lambda_{2b} v^2}{2} \end{pmatrix}, \quad (2.3)$$

The eigenvalues of this matrix can be easily calculated:

$$\begin{aligned}
(m_{s_1^0, s_2^0})^2 &= \frac{1}{4} \left(2(M_{S_1}^2 + M_{S_3}^2) - (\lambda_2 + \lambda_{3a}) v^2 \right. \\
&\quad \left. \mp \sqrt{(2(M_{S_1}^2 - M_{S_3}^2) + v^2(\lambda_{3a} - \lambda_2))^2 + 8\lambda_5^2 v^4} \right), \quad (2.4)
\end{aligned}$$

The mixing angle between the neutral states is given by:

$$\tan 2\theta = \frac{\sqrt{2}\lambda_5 v^2}{(M_{S_3}^2 - M_{S_1}^2) + \frac{1}{2}(\lambda_2 - \lambda_{3a})v^2}. \quad (2.5)$$

This mixing angle between t_0 and S_0 is usually small (unless $M_{S_1}^2 \equiv M_{S_3}^2 - v^2(\lambda_{3a} - \lambda_2)/2$, where the denominator of eq. (2.5) becomes zero), since typically $\lambda_5 v^2 \ll M_{S_1}^2, M_{S_3}^2$. For $M_{S_1} \leq M_{S_3}$ the lighter of the neutral scalars, s_1^0 , is mostly a singlet while $s_2^0 \simeq t^0$. In a slight abuse of notation, we will call the lightest neutral scalar, s_1^0 , simply S_0 from now on.

On the other hand, the masses of the charged components of the scalar triplet t^{++} and t^+ are:

$$\begin{aligned}
m_{t^{++}}^2 &= M_{S_3}^2 - \frac{1}{2}(\lambda_{3a} + \lambda_{3b})v^2, \\
m_{t^+}^2 &= M_{S_3}^2 - \frac{1}{4}(2\lambda_{3a} + \lambda_{3b})v^2.
\end{aligned} \quad (2.6)$$

We will be interested in studying DM in this model, thus typically the lightest neutral state will be mostly singlet with some (small) admixture from t_0 .⁴

⁴A pure t_0 is not a good DM candidate, due to constraints from direct detection experiments [27].

For completeness, we mention that due to the Z_2 symmetry the vector-like fermions do not mix with the SM leptons. The charged and the neutral member of F are not exactly degenerate, since 1-loop corrections from QED affect the mass of F^+ but not F^0 . This mass splitting is of order 0.3 GeV [34], sufficiently large that the decay $F^+ \rightarrow \pi^+ + F^0$ is always kinematically possible.

The model generates 1-loop neutrino masses from diagram T-3 of [22]. The neutrino mass matrix is given by:

$$m_\nu = \mathcal{F} \left(h_F^T \hat{M}_R h_{\bar{F}} + h_{\bar{F}}^T \hat{M}_R h_F \right). \quad (2.7)$$

Here $\mathcal{F} \sim \frac{1}{2} \frac{\sin 2\theta}{16\pi^2}$ and \hat{M}_R is a (3×3) matrix with diagonal entries given by:

$$(\hat{M}_R)_{ii} = \Delta B(x_i, y_i) m_{F_i}, \quad (2.8)$$

with $x_i = ((m_{s_1^0}/m_{F_i})^2)$, $y_i = ((m_{s_2^0}/m_{F_i})^2)$, $m_{s_i}^0$ the eigenvalues of Eq. 2.3 and

$$\Delta B(x, y) = \frac{x \log(x)}{x-1} - \frac{y \log(y)}{y-1}. \quad (2.9)$$

As shown in eq. (2.7) the neutrino masses depend on the product of two h_F , $h_{\bar{F}}$ Yukawa couplings, which in principle can be different. Fits to neutrino data of the parameters in eq. (2.7) can be done using the master parametrization [35]. Since we will not study flavour in detail in this paper, we use a simplified version of the general formula in our fits. This simplification does not affect the decay length nor the DM calculation. In these fits, we express h_F in terms of the measured neutrino masses and angles, the fermion mass eigenvalues m_{F_i} and $h_{\bar{F}}$, which we choose randomly, resulting in:

$$h_F = \frac{1}{2\mathcal{F}} \hat{M}_R^{-1} (h_{\bar{F}}^T)^{-1} U_\nu^* \hat{m}_\nu U_\nu^\dagger, \quad (2.10)$$

where $[M_R] = [\text{GeV}]$, $[m_\nu] = [\text{eV}]$, while the Yukawa couplings h_F and $h_{\bar{F}}$ are adimensional. Here, \hat{m}_ν are the light neutrino mass eigenvalues ($m_{\nu_i} = m_{\nu_1}$, $\sqrt{\Delta(m_{sol}^2) + m_{\nu_1}^2}$, $\sqrt{\Delta(m_{atm}^2) + m_{\nu_1}^2}$), with $\Delta(m_{sol}^2)$ and $\Delta(m_{atm}^2)$ the solar and atmospheric mass squared splittings and U_ν is the neutrino mixing matrix, measured in oscillation experiments.

We note that the values of λ_5 that we use in our numerical analysis are compatible with neutrino oscillation data and also with current upper limits on charged lepton flavor violating (cLFV) decays, such as $\mu \rightarrow e\gamma$. Avoiding significant cLFV observables can be achieved in different ways. The two simplest possibilities are: i) Choosing a large enough value of λ_5 , which, see eq. (2.7), results in $h_F \ll 1$ and $h_{\bar{F}} \ll 1$ in the neutrino fit. In this scenario, the model clearly satisfies cLFV constraints. ii) Choosing either h_F or $h_{\bar{F}}$ to be diagonal and order $\mathcal{O}(1)$. This then automatically leads to non-diagonal yukawa couplings $\ll 1$, thus cLFV constraints are fulfilled again. In our model, cLFV current bounds are always irrelevant for values of λ_5 larger than $\lambda_5 > 10^{-6}$. In our numerical analysis, we do not consider values of λ_5 smaller than this value.

2.2 Model implementation and decay widths

We implemented the model into SARAH [36, 37]. SARAH automatically generates **SPheno** routines [38, 39] for the numerical calculation of the mass spectra, mixing matrices, scalar and fermionic two-body decays, and other observables. SARAH also generates model files for **MicroMegas** [40], with which we calculate the relic density and the direct detection cross section for our dark matter candidate. UFO input files for **MadGraph** [41, 42] can also be generated, which we then use for the calculation of 3-body, 4-body and 5-body decay widths of the exotic scalars, as well as for the production cross sections.

With hindsight of the results in sections 3 and 4, we will next briefly describe scalar decay widths. Here, we will assume that the fermions have masses larger than t^{++} and $m_{t^{++}} - m_{t^+} \leq m_W$, such that there are no two-body decay channels allowed kinematically for t^{++} . The doubly charged component of the scalar triplet will decay to the lightest neutral scalar, usually mostly a scalar singlet (and the dark matter candidate of the model), and either two charged leptons or two W^+ -bosons, via the diagrams shown in the top line of fig. 2. If the mass splitting, $\Delta m \equiv m_{t^{++}} - m_{S_0}$, is smaller than $2m_W$ (m_W), at least one of the W^+ s will be off-shell and the decay $t^{++} \rightarrow W^+ + (W^+)^* + S_0$ becomes effectively a 4-body (5-body) decay, as shown in the diagrams in the second line of fig. 2.

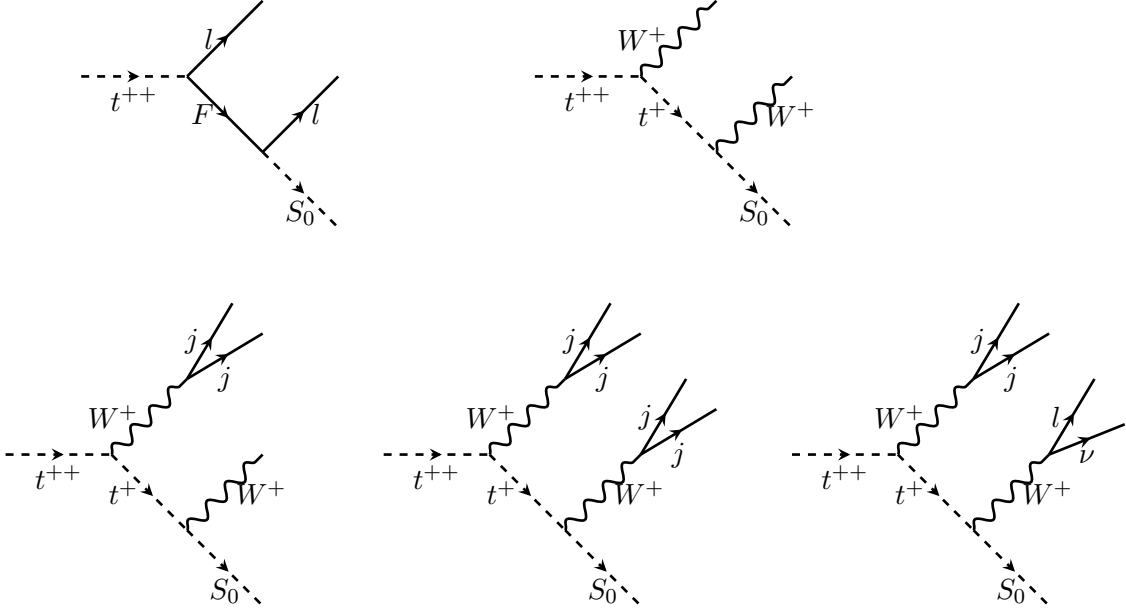


Figure 2. Example Feynman diagrams for t^{++} decays. The diagrams in the first line show 3-body decays, while the diagrams in the bottom line show the corresponding 4- and 5-body decays, if the mass splitting between the t^{++} and the dark matter candidate is smaller than $2m_W$ and m_W , respectively.

The W^+ themselves can either decay leptonically or hadronically, thus the 5-body final states can be either $4j + S_0$, $2jl\nu + S_0$ or $2l2\nu + S_0$. We define $\Gamma_l = \Gamma(t^{++} \rightarrow l^+ + l^+ + S_0)$ and $\Gamma_{had} = \Gamma(t^{++} \rightarrow 4j + S_0) + \Gamma(t^{++} \rightarrow 2j + l\nu + S_0)$. Note that the final state $2l2\nu + S_0$

(mediated by W s) can not be easily distinguished from $2l + S^0$, due to the missing energy (from the S^0) in the events.

For the collider phenomenology the total decay length of t^{++} is important. We can essentially distinguish three regimes: prompt decays ($c\tau \lesssim \mathcal{O}(1)$ mm), finite lengths, $c\tau \sim$ (mm - m), or quasi-stable events ($c\tau \gtrsim \mathcal{O}(10)$ m). In fig. 3 we show some example decay widths of t^{++} as a function of Δm , for different choices of λ_5 and M_{S_3} . Note that in this figure we always fit neutrino masses such that they reproduce oscillation data (for normal hierarchy). This leads to a fixed choice of $h_F h_{\bar{F}}$, once λ_5 and m_F are fixed.

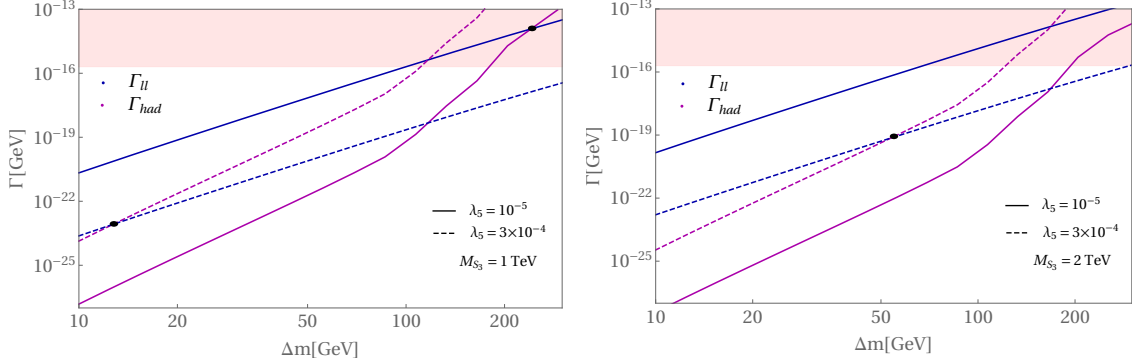


Figure 3. Decay width as a function of Δm for different values of λ_5 . The left (right) panels correspond to $M_{S_3} = 1$ TeV ($M_{S_3} = 2$ TeV). The amplitudes Γ_{ll} and Γ_{had} refer to $\Gamma(t^{++} \rightarrow l^+ + l^+ + S_0)$ and $\Gamma(t^{++} \rightarrow 4j + S_0) + \Gamma(t^{++} \rightarrow 2j + l\nu + S_0)$ respectively. The pink band corresponds to the region where $c\tau$ of t^{++} corresponds to the “displaced” regime, i.e $c\tau \sim$ (mm - m). For this figure we have fixed $m_F = 2.5$ TeV.

As fig. 3 demonstrates, which of the final states, “hadronic” (whose width we define as Γ_{had}) or “leptonic” (whose width we define as Γ_{ll}), dominates the decay width depends mostly on the choice of λ_5 – and to a lesser extend – on Δm and M_{S_3} .⁵ Generically, for λ_5 larger than (few) 10^{-4} the hadronic channel will dominate the decay of t^{++} , regardless of other model parameter choices, unless Δm is very small (say, $\Delta m \simeq$ (few) GeV), where a strong phase space suppression for the 5-body decays occurs. The exact value of Δm , where Γ_{had} becomes larger than Γ_{ll} depends on M_{S_3} of course, but larger Δm prefers the hadronic channels (since Γ_{had} has a stronger dependence on Δm than Γ_{ll}).

Very generally, the decay width of t^{++} is expected to be a very small number, essentially because the smallness of neutrino masses require that the product $\lambda_5 h_F h_{\bar{F}}$ is small. Note that large part of the parameter space shown in fig. 3 actually leads to widths that are so small that the t^{++} becomes quasi-stable. In this case the t^{++} will leave a track in the LHC detectors, but the final states are not accesible, of course.

⁵There is not much dependence on m_F , since a choice of a larger m_F is partially compensated by a larger $h_F h_{\bar{F}}$ from the neutrino mass fit.

3 Dark matter phenomenology

The presence of a preserved Z_2 symmetry in the SST model implies that the lightest Z_2 -odd particle is completely stable, hence a potential DM candidate. Among the possible fermionic and scalar particles, we focus on the scenario where S_0 is the lightest Z_2 -odd state. As aforementioned, S_0 is a CP-even mass eigenstate resulting from the mixing between the neutral components of the singlet and triplet scalars. Under the assumption $M_{S_3}^2 > M_{S_1}^2$, S_0 will typically be the lightest scalar for most values of the quartic couplings λ_i , provided they remain perturbative. Moreover, if λ_5 is small, the S_1 - S_3 mixing is suppressed and S_0 will be predominantly the real scalar singlet S_1 . Therefore, it inherits some properties of singlet scalar DM candidates [43–46]. Additionally, we assume that $m_F^2 > M_{S_1}^2$, ensuring that the vectorlike leptons remain heavier than S_0 . Throughout our analysis, we enforced these conditions and considered points in the parameter space where S_0 is the lightest Z_2 -odd particle.

The S_0 relic abundance Ωh^2 can be generated within the standard thermal WIMP paradigm, leading to [47]

$$\Omega h^2 = \frac{1.09 \times 10^9 \text{GeV}^{-1}}{g_*^{1/2} M_{PL}} \frac{1}{J(x_f)}, \quad (3.1)$$

where g_* denotes the number of relativistic degrees of freedom at freeze-out, $x_f = m_{S_0}/T_f$ and

$$J(x) = \int_x^\infty \frac{\langle \sigma v \rangle}{x^2} dx, \quad (3.2)$$

with $\langle \sigma v \rangle$ being the thermal average of the DM annihilation cross section. For a hierarchical spectrum of Z_2 -odd scalar particles, the primary annihilation channels contributing to $\langle \sigma v \rangle$ stem typically from Higgs mediated processes controlled by the quartic couplings, most prominently λ_2 , which couples S_1 to the Higgs doublet H . Contributions from terms proportional to λ_{3a} and λ_{3b} , which link S_3 to H , are also significant, though less relevant in the limit of small S_1 - S_3 mixing. As these quartic couplings also set the strength of DM-nucleus scattering cross section, dominated by t -channel Higgs exchange, this scenario of DM production driven by Higgs portal couplings faces strong constraints from current direct detection searches [27, 28].

When the mass splitting between the singlet and triplet scalars is not significantly large, however, co-annihilation channels involving t^{++} , t^+ , t^0 come into play and dominate $\langle \sigma v \rangle$. The importance of co-annihilation processes becomes substantial when the relative mass splittings of the triplet scalars with S_0 are much less than 1 [47]. In this case, λ_5 and Δm become the key parameters in determining the DM relic abundance. This is demonstrated in fig. (4) for some specific example. Co-annihilation allows the correct Ωh^2 to be obtained in a broader range of S_0 masses.

In fig. 5 the DM relic abundance is calculated for the two different scenarios described above, i.e., the hierarchical scalar spectrum (left panel), and compressed scalar spectrum (right panel). In these plots, the quartic couplings are fixed as $\lambda_2 = \lambda_{3a} = \lambda_{3b} = 10^{-3}$, while

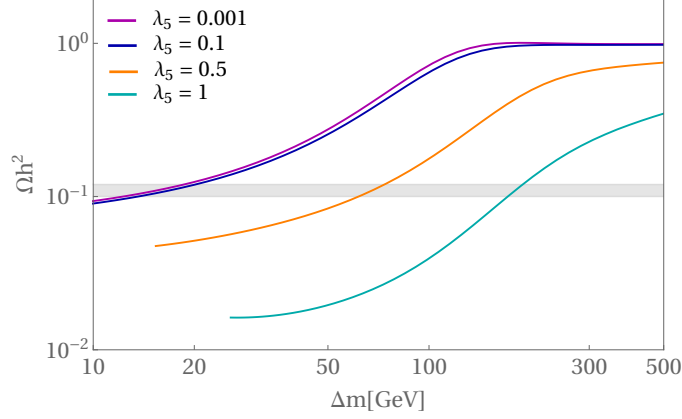


Figure 4. The plot shows Ωh^2 as function of Δm for four different choices of λ_5 for one fixed, but arbitrary choice of $m_{S_0} = 1$ TeV. Smaller values of λ_5 lead to smaller mixing between the neutral singlet and triplet states and, thus to a larger Ωh^2 . However, even for very small λ_5 , the correct Ωh^2 can be achieved if Δm is small. The plot therefore demonstrates the importance of coannihilation.

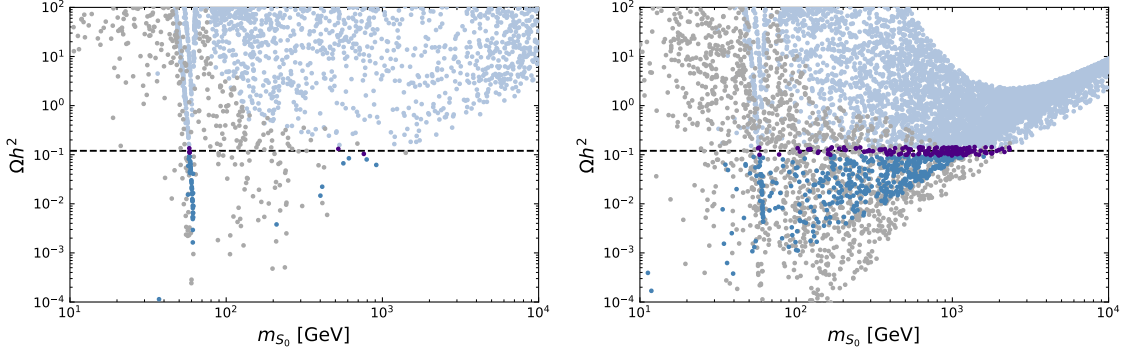


Figure 5. Dark matter relic density in the non-coannihilation (left panel) and coannihilation (right panel) regimes (see the text). Violet points comply with the relic density value as measured by Planck. The grey points are excluded by direct detection constraints, while blue (light blue) points pass the direct detection bound, but yield underabundant (overabundant) DM. Note that the presence of coannihilation allows many viable points for m_{S_0} in the range of hundreds GeV to few TeV.

the other parameters are varied randomly in the following ranges: $m_{S_0} \in [10 \text{ GeV}, 10 \text{ TeV}]$, $\lambda_5 \in [10^{-4}, 1]$, $\Delta m \in [0, 5 \text{ TeV}]$ (in the left panel) and $\Delta m \in [0, 200 \text{ GeV}]$ (in the right panel). m_F varies in the same range as m_{S_0} , however always respecting the condition $m_F > m_{S_0}$. In the numerical analysis, we utilized the **MicrOmegas v5.2.4** package [40] to compute the DM abundance and also to compute the scattering cross section for direct detection. Additionally, consistency with neutrino oscillation data was enforced by the use of Eq. (2.10), for which a fixed value of $h_{\bar{F}} = 10^{-2}$ has been chosen for the Yukawa couplings.

As can be seen in the left panel of fig. 5, in the hierarchical spectrum scenario the

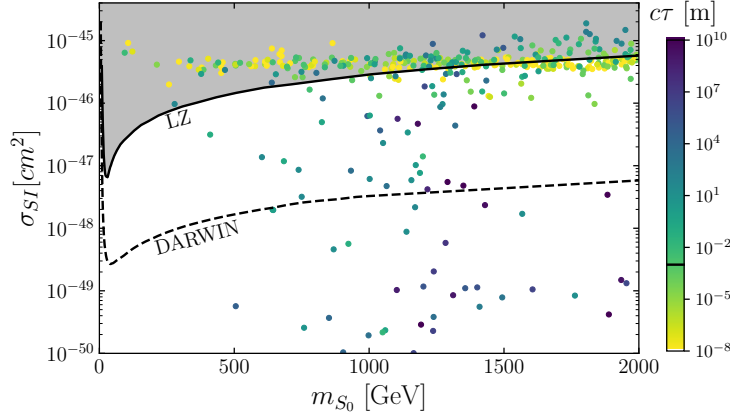


Figure 6. Spin-independent DM direct detection cross section versus DM mass. The sidebar indicates the lifetime of the t^{++} scalar, with bluish (yellowish) points corresponding to long-lived (short-lived) t^{++} . The strip in the sidebar corresponds to $c\tau = 1$ mm, which is the threshold above which we consider a particle to be long-lived. The t^{++} particle is long-lived for the majority of points that satisfy current direct detection constraints, including *all* the points that evade future detection by DARWIN.

majority of points that reproduce the correct relic density are excluded by LUX-ZEPLIN (LZ) data [27], except for small regions where m_{S_0} is around $m_h/2$ (the Higgs resonance) or within the restricted interval between 500-800 GeV. Larger m_{S_0} values fail to generate the correct Ωh^2 for the chosen fixed values of $\lambda_{2,3a,3b}$. Even though we could allow heavier S_0 by making $\lambda_{2,3a,3b}$ larger, these points would be ruled out by direct detection, as the increase in the couplings lead to larger DM-nucleus scattering cross-section, mediated by the Higgs. Besides, this setting is less attractive from the phenomenological point of view, as the extra particles tend to be heavier than TeV, making their search at colliders a difficult task.

As the hierarchical scenario is severely constrained by direct detection, we turn our attention to the alternative case, shown in the right panel of fig. 5. In this plot, the mass splitting is restricted to be less than 200 GeV, so most of the points fall within the co-annihilation regime. In this situation, the additional channels enhance the annihilation efficiency without the need of increasing the Higgs portal couplings. Consequently, the relic density is correctly generated over a broader range of m_{S_0} values, including small masses of the order of a few hundred GeV, while evading direct detection constraints. Note that if S_0 is light, the small mass splitting implies that the other scalars are also light, and hence can potentially be produced at the LHC.

An additional feature that emerges in the co-annihilation regime, favored by DM, is the fact that the doubly charged scalar t^{++} is typically long-lived. This is illustrated in fig. 6, where the DM direct detection cross section is plotted against the DM mass, with the sidebar showing the decay length of t^{++} . In this scan, all the points comply with the Planck constraint $\Omega h^2 = 0.1200 \pm 0.0036$ (at 3σ) [26], and the neutrino mass fit as described previously. The quartic couplings are allowed to vary in the range $\lambda_i \in [10^{-6}, 1]$,

and Δm varies from 0 to 500 GeV. As m_{S_0} in the horizontal axis goes up to 2 TeV, we fixed $m_F = 2.5$ TeV. It is apparent that the points currently allowed by LZ bounds are mostly bluish, which means that t^{++} has a macroscopic $c\tau$. These points correspond to regions of the parameter space in which Δm is small, i.e., they are in the co-annihilation regime. Some of these points are within reach of future direct detection experiments, which could lead to signals in more than one kind of experiment. Other points, however, escape the sensitivity even of “ultimate” detectors, such as DARWIN [24, 48]. This part of the parameter space can still be probed at colliders, especially by taking advantage of the long lifetime of t^{++} . Note, in particular, that all the points that evade future detection by DARWIN feature a long-lived t^{++} , leading to $c\tau \gtrsim 10$ m. This is why we focus on the long-lived particle signatures in the following section.

4 Collider phenomenology

We study the collider signatures of the multi-charged candidate, t^{++} , which can have lifetimes ranging from the prompt regime to several hundreds of meters. Figure 7 shows the lifetime dependence on the relevant model parameters for collider phenomenology⁶: λ_5 and $\Delta m \equiv m_{t^{++}} - m_{S_0}$, as a function of the proper decay distance of t^{++} , $c\tau$. Points where the decay width to hadrons (Γ_{had}) is dominant are shown in purple circles⁷.

Macroscopic values of $c\tau$ starting from 1 mm and above – for points that survive constraints from direct detection – are achieved for values of λ_5 roughly smaller than $\sim 10^{-1}$ and $\Delta m \lesssim 50$ GeV. For larger values of Δm points could still lie within the “finite” $c\tau$ range (for $c\tau$ between 1 mm and 1 m, considering the acceptance of the ATLAS inner tracker detector), but then most of these points are excluded by direct detection experiments, as shown in the left panel of figure 7.

While some points in the prompt regime are still allowed by LZ, DARWIN would exclude them. This is why we do not consider collider constraints from prompt searches, as these points would already be excluded by future direct detection experiments (see also figure 6). We therefore focus on long-lived particle (LLP) searches because the reach is much bigger there than for the prompt case. In principle the LLP decay modes of t^{++} include several 3-body and 5-body final states to DM, charged leptons, neutrinos and jets (see section 2). We choose to focus on the delayed hadronic decay signatures of the t^{++} (Γ_{had} , see figure 3) at the LHC. Although we expect the reach in the leptonic channel (when considering Γ_{ll}) to be similar, we in fact expect a smaller reach with displaced leptons, when compared to displaced vertex searches in hadronic channels, where the vertex is made from charged particle tracks coming from quark hadronization [49]. This can be expected due to larger backgrounds [50, 51] and/or softer displaced leptons [52, 53], leading to smaller

⁶We fix for definiteness the mass of all heavy fermions to $m_F = 2.5$ TeV, while $\lambda_2, \lambda_{3a} = \lambda_{3b}, \lambda_{6a} = \lambda_{6b}$ and λ_7 are free in what follows.

⁷For these points, the leptonic decay mode is suppressed, meaning, $\text{BR}(t^{++} \rightarrow l^+ + l^+ + S_0) < 0.1$

efficiencies⁸. We therefore choose to study the hadronic channel in detail.

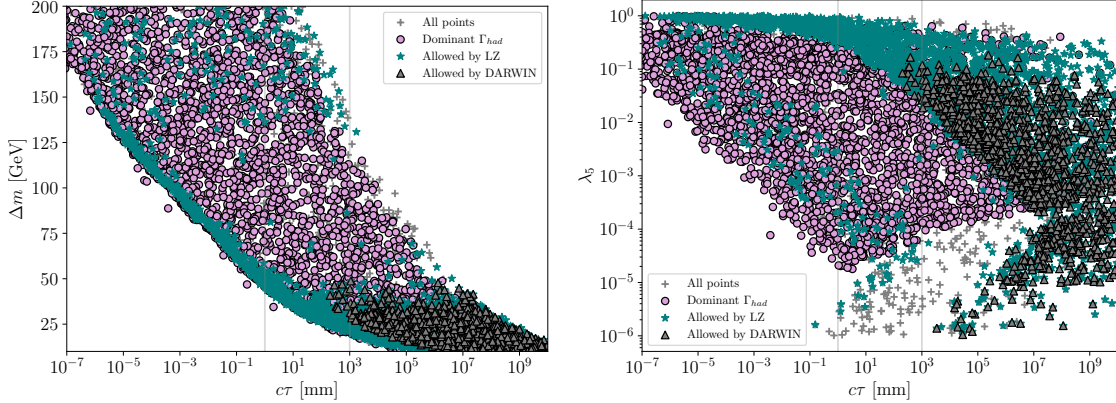


Figure 7. Proper decay distance $c\tau$ as a function of Δm (left panel), and λ_5 (right panel). All scanned points are represented in grey (with a cross) on the background. Points where the decays to hadronic Γ_{had} dominates are shown in purple circles. We also overlay points satisfying the LUX-ZEPELIN (LZ) bound with a green star and DARWIN with a grey triangle. The “finite” $c\tau$ range is represented as vertical lines for $c\tau = 1$ mm and $c\tau = 1$ m.

Displaced vertex (DV) searches [54, 55] and searches for multi-charged particles [56] will be sensitive to test the model at the LHC in its high-luminosity phase in the “finite” $c\tau$ range i.e. $\sim \mathcal{O}(1\text{mm} - 1\text{m})$ and the “larger” lifetime regime i.e. $c\tau \gtrsim \mathcal{O}(10\text{m})$, respectively⁹. We consider the LHC production in `MadGraph5_aMC@NLO` v3.5.1 [42, 59] of t^{++} at $\sqrt{s} = 13$ TeV, $pp \rightarrow t^{++}t^{--}$, with model spectra calculated from `Spheno`. We use the `LUXqed17_plus_PDF4LHC15_nnlo_100` parton distribution function set obtained from LHAPDF-6.2.3 [60] to accurately account for photon-fusion diagrams. Generated events are then interfaced to `Pythia8` [61] for showering and hadronization. Missing transverse momenta, jets (with the help of `FastJet3.3.2` [62]) and displaced vertices are also reconstructed within `Pythia8`, following a custom made code with displaced efficiencies validated for the ATLAS DV search previously in refs [63, 64].

We start by reinterpreting two ongoing searches¹⁰ targeting the finite and large $c\tau$ regions: i) The ATLAS 13 TeV “DV+MET” search [54] and the latest ii) ATLAS search for multi-charged particles [56].

⁸Although we note in our model the leptons are not always soft, as Δm could be large enough for the displaced lepton’s transverse momentum to pass the trigger selections.

⁹Similar signatures for long-lived multi-charged particles predicted in neutrino mass models were studied in [57, 58].

¹⁰In principle, searches for disappearing charged tracks [65, 66] could also constrain these types of models (see for instance an example in the Scotogenic model in [11, 67]). Nevertheless, our phenomenology is more complex, as with a doubly charged LLP, the mass difference between the LLP and DM is large enough for our final state jets to be fully visible. We in addition have 5-body decays. We have checked for example constraints to our model from LLP searches contained within `SmodelS` [67], and find it is not covered by any of the simplified model topologies. We thank Andre Lessa for his help in identifying this.

- i) The ATLAS 13 TeV “DV+MET” search [54] was first validated in [64] by some of us. The signature includes at least one displaced vertex in association with large missing transverse momenta, used as a trigger. Following the recast prescription in the auxiliary material of the search [68], our event selection starts with the reconstruction of missing transverse momenta at the truth level, $p_T^{\text{miss}} > 200$ GeV, which considers all stable and neutral BSM particles and SM neutrinos. We then require either one or two trackless jets with $p_T > 70$ GeV or $p_T > 25$ GeV, respectively. A trackless jet is a jet with a scalar sum of the p_T of all of its charged particles inside it to be less than 5 GeV. Following the prescription, these jet requirements are applied to 75% of the events. We then apply cuts imposed on events with displaced vertices reconstructed from displaced tracks: displaced vertex coordinates within $4 \text{ mm} < r_{\text{DV}} < 300 \text{ mm}$ and $|z_{\text{DV}}| < 300 \text{ mm}$, number of final state charged tracks coming from the vertex to be at least 5 (each with $p_T > 1$ GeV and $|d_0| > 2 \text{ mm}$), and invariant mass larger than 10 GeV (reconstructed assuming all tracks have the pion mass). We assume zero background, ensured by the large track multiplicity and invariant mass requirements of the displaced vertex. In some of our search proposals in what follows, we tune the trigger cut and require a lower threshold of $p_T^{\text{miss}} > 50$ GeV, while the displaced activity cuts remain the same as the original search.
- ii) ATLAS also searched for multi-charged particles in ref. [56]. The search is also essentially background free for electric charges of $z \geq 2$ and $c\tau \gtrsim 10 \text{ m}$. For the recast, we compare our cross-section results with the upper-limits presented by ATLAS in fig. 8 of ref. [56], which shows the production cross-section as a function of mass for doubly charged particles. We estimate a lower limit on t^{++} to be $m_{t^{++}} \gtrsim 800 \text{ GeV}$ for $\mathcal{L} = 136 \text{ fb}^{-1}$. As this search is essentially background free, we can estimate the future sensitivity by just scaling the existing limit with the expected luminosity gain. With this we get a lower limit of $m_{t^{++}} \gtrsim 1240 \text{ GeV}$ at $\mathcal{L} = 3000 \text{ fb}^{-1}$.

Figure 8 shows our “DV+MET” reinterpreted limits in the plane $c\tau$ vs. $m_{t^{++}}$, by requiring 3 signal events (which correspond to 95 % C.L. exclusion limits under zero background). The left panel shows in orange our straightforward recast at $\mathcal{L} = 32.8 \text{ fb}^{-1}$. We also extrapolate our limits to $\mathcal{L} = 300 \text{ fb}^{-1}$ with blue lines, considering a proposal for a lower trigger threshold on missing transverse momenta of 50 GeV (instead of the original trigger of $p_T^{\text{miss}} > 200 \text{ GeV}$). In principle a tuning of the search cuts would require a proper experimental study of backgrounds, which is beyond the scope of this work. Nevertheless, our unique model signature consists of a doubly charged long-lived particle that can decay inside the trackers of LHC detectors¹¹, and so the charged activity or passage through the detector can be further used to reconstruct additional observables such as large-ionization energy (similar as for multi-charged particle searches [56, 69] for instance) in order to

¹¹Note that signal model benchmarks in searches for displaced vertices [54, 55] usually target neutral long-lived particles, so our signature is not exactly covered by ongoing searches.

eliminate possible background sources by enforcing additional displaced activity¹². This motivates further experimental studies by the LHC collaborations particularly at the high-luminosity phase of the LHC. The right panel in figure 8 shows our DV projections for $\mathcal{L} = 3000 \text{ fb}^{-1}$ in orange lines, as well as the proposed search with $p_T^{\text{miss}} > 50 \text{ GeV}$. Masses of $t^{++} \sim 1.5 \text{ TeV}$ can be probed with this proposed optimization (about 300 GeV higher than what is achievable by projecting the limit of the original search). We also overlay in figure 8 derived limits from multi-charged searches in the pink region, which are sensitive to higher lifetimes for $c\tau > 10 \text{ m}$ and so complementary to searches for displaced vertices, which yield the strongest upper limit roughly at $c\tau \sim 10 \text{ cm}$.

We also highlight that in figure 8, solid lines assume a 100% branching ratio to final states containing hadronic modes (i.e. $\Gamma_{\text{had}}/\Gamma$). This decay mode allows for plenty of final state visible tracks so that the multi-track displaced vertex search is applicable and efficient. We also present a conservative choice of 50% branching ratio in dashed lines.

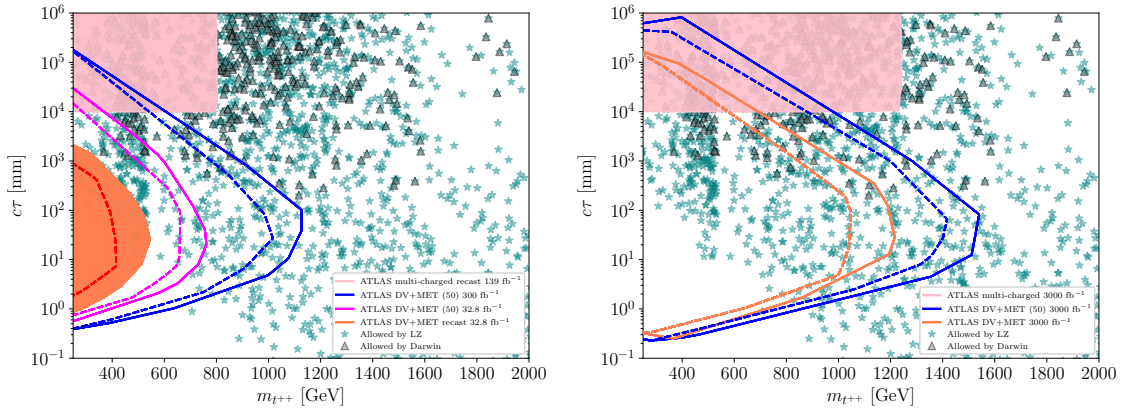


Figure 8. Projected LHC limits in the $m_{t^{++}}$ vs. $c\tau$ plane for long-lived particle searches with displaced vertices (solid and dashed lines), and multi-charged particles (pink shaded regions) for “current” luminosities (left panel) and the higher-luminosity phase of the LHC (right panel). Solid lines assume 100% branching ratio of $\Gamma_{\text{had}}/\Gamma$ and dashed lines a 50%. Points satisfying the LUX-ZEPELIN (LZ) bound are marked with a green star and the ones satisfying DARWIN with a grey triangle.

From our results in figure 8 we draw that dark matter masses m_{S_0} of $\mathcal{O}(1) \text{ TeV}$ can be reached in the most optimistic scenario (blue solid line, left panel) at current LHC stages of the luminosity. This goes up to $\sim 1.4 \text{ TeV}$ at 3000 fb^{-1} (blue solid line, right panel). Also, points that could be probed by multi-charged searches at the LHC could also be tested at future dark matter direct direction experiments as DARWIN. Points with dark matter masses above $\sim 1.4 \text{ TeV}$ and $\lambda_5 \lesssim 10^{-2}$ would still be allowed by DARWIN.

¹²A similar direction for such an optimization in the context of Heavy Neutral Leptons was proposed in ref. [70] by requiring a displaced trigger at CMS, which allowed for a lower p_T^{miss} threshold.

5 Summary and discussion

In this paper we have studied the phenomenology of a neutrino mass model, which we called SST for short, that explains at the same time the dark matter problem. We have demonstrated that it is possible to explain the relic density of DM and at the same time obey all existing bounds from direct detection in this model. We note that the combination of the different DM constraints favours a parameter region, where the mass splitting between the scalar singlet and triplet is much smaller than their average mass $\Delta m/m \ll 1$, such that there is at least some contribution from co-annihilation processes in fixing of the relic density. In this parameter region, the doubly charged member of the triplet, t^{++} , typically has a very small decay width.

The particular model variant considered in this paper, differs from the famous *scotogenic* model [1, 2] in that it has a much richer collider phenomenology. It is but one example in a rather lengthy list of such one-loop neutrino mass DM models given in [23], albeit, as discussed below, most or all of the collider signals we considered in this paper will be present in many of the other models in this model class as well. We stress again, that one can consider the scotogenic model the proto-type in a class of models that at the same time can explain neutrino masses and dark matter, but *all* models in this class can do so. The motivation to study collider phenomenology arises from the fact that the observation of a signal at the LHC (or any other future collider) might be the only way to distinguish between all that plethora of model variants.

Both, the neutral component of the fermion multiplet as well as the lighter of the neutral scalars can be the DM, in principle. In this work, we have concentrated on the case of the scalar being the DM (assuming that all fermions in the model are heavier than the scalar states). The motivation for this choice is twofold. First, direct detection constraints would rule out the neutral component of a $F_{1,2,1/2}$ as DM unless a ($d = 5$) non-renormalizable operator is added to the model such that the fermion becomes "inelastic" dark matter [25]. To explain such a NRO, with the required size, would need an additional (particle) extension of the model. Second, as discussed in the previous section, searches for long-lived and/or quasi-stable particles are particularly promising in their mass reach. While multiply charged scalars can have, in principle, any decay length, for a charged fermion (member of a $SU(2)_L$ multiplet) the situation is different. QED corrections split the masses of the charged and the neutral fermions, such that the charged fermion will always decay to the neutral fermion one plus a (very soft) charged pion [34]. This gives an upper limit on the decay length of charged fermions of at most a few cm for $SU(2)_L$ doublets (and much smaller lengths for members of larger $SU(2)_L$ multiplets) [57].

The phenomenology of multiply charged scalars depends on their decay width. t^{++} can decay either promptly, with a displaced vertex (DV+MET search) or be quasi-stable (decay lengths larger than the size of the detectors). Reinterpretation of existing DV+MET searches [54, 55] leads to lower mass limits of order $\mathcal{O}(500 - 600)$ GeV, see fig. 8. We then extrapolate these results to higher luminosities, projecting future limits in the range

1.2 – 1.5 TeV for 3000 fb^{-1} . A reinterpretation of ATLAS [56] search for quasi-stable multiply charged states allows us to estimate a lower limit on the mass of t^{++} to be around 800 GeV, based on a luminosity of 136 fb^{-1} . With $\mathcal{L} = 3000 \text{ fb}^{-1}$ this limit could be improved up to 1.2 TeV.

As mentioned above, a comprehensive list of 1-loop neutrino mass models that can also explain DM has been given in [23], encompassing a total of 318 model variants. This large number prompts the question whether the conclusions drawn in this article are applicable also to other models in this list. Before closing, we would like to discuss this question at least briefly, though only qualitatively.

First, we note that multiply charged scalars are a general feature in this model class. From the 318 models, listed in the appendix of [23], 291 models contain multiplets with a maximum charge of at least two. Even restricting ourselves only to the more minimal set of models of table 8 of [23],¹³ we note that $S_{1,3,1}$ appears in 22 models, while 65 of the 91 models listed have doubly charged scalars, 18 of these models have a triply charged scalar and there are even 2 models for which the largest electric charge is actually 4.

The phenomenology of the doubly charged scalars will, in principle, always be similar to what we discussed in this paper. In all cases the decays of these states will contain either $WW + \text{MET}$ or two same-sign leptons plus MET. Again, depending on the mass splitting between S^{++} ¹⁴ and the DM candidate, S^0 , the W -bosons could be on-shell or off-shell. In general, unless the singly charged scalar (which must always be present too in models with doubly charged states) is lighter than the S^{++} , one expects the S^{++} to be long-lived or quasi-stable, similar as in the SST model. Production cross sections depend not only on the electric charge but also on the $SU(2)_L$ multiplet, but for larger multiplets than the triplet considered in this paper, larger production cross sections are expected and, thus, the sensitivity reach of the LHC for these should be correspondingly larger.

Cross sections at the LHC generically increase with electric charge. For scalar states with similar masses one therefore always expects that the state with the largest charge will be produced most abundantly. Decay widths of scalars, on the other hand, become drastically smaller with increasing electric charge. Here, two effects are important. First, n -body phase spaces become smaller with increasing n . And, second, in case of $n * W$ final states, the available phase space, determined by $\delta m = m_{S^{n+}} - m_{S^0} - nm_W$, will lead to a strong suppression of the width (for $\Delta m/m \ll 1$, as discussed above). For triply or even quadruply charged states one can therefore expect that large parts of the parameter space in these neutrino mass models, allowed by DM constraints, will lead to quasi-stable scalars. The ATLAS search [56] shows *increasing* sensitivity to states with larger electric charges, thus we can expect better sensitivities than what we found in the SST model for models with highly charged scalars.

¹³Tables 9 and 10 contain models with larger representations and hypercharges, which lead to even larger electric charges and production cross sections, but admittedly look more contrived theoretically.

¹⁴We use here S^{++} , to indicate any scalar with two electric charges, to differentiate from t^{++} , which is the doubly charged member of a triplet.

How can we distinguish between neutrino mass models in this list using the LHC? Singling out *any* particular model will be hard. Since it is possible to determine the electric charge of long-lived scalars, one could start to exclude models based on this rather straightforward observation: The scotogenic model has no doubly charged particle, thus the observation of a S^{++} disfavors it. Observation of a triply charged and a doubly charged scalar would rule out many more models and so on. However, if any of the signals studied in this article, such as displaced vertices or multi-charged particles, were to be observed, it would serve at least as a hint towards one of these models. Additional information would be necessary to establish a direct connection. For instance, in the case of signals with displaced vertices where scalars decay within the detector, detecting different decay modes ($WW + \text{MET}$ and two same-sign leptons + MET) would certainly help towards identifying the underlying model.

This paper is mostly concerned with the determination of the parameter space, where the t^{++} predicted by our model could be discovered at the LHC. Before closing, we would like to discuss briefly the question, whether such a discovery could actually be used to demonstrate that the neutrino mass generation mechanism has been identified *experimentally*.

All Majorana neutrino mass models violate lepton number. Thus, it seems straightforward: Demonstrate that the particle discovered has both, a lepton number conserving (LNC) and a lepton number violating (LNV) decay mode. However, given the finite statistics expected even for $\mathcal{L} = 3/\text{ab}$, this requires that the hadronic and leptonic final states of the t^{++} decay have very similar branching ratios, otherwise only one of the two will be observable. As fig. (3) shows, parameter points with $\Gamma_{ll} = \Gamma_{had}$ exist. However, it is also obvious that the ratio of these two widths can differ widely. Thus, the discovery of lepton number violation is not guaranteed, even if the t^{++} is found at the LHC.

Even if both decay modes were measured at the LHC, there is the problem that all final states contain a DM particle, i.e. experimentally missing energy. LNV can not be easily established in events with missing energy. To demonstrate that the missing energy is not due to emission of neutrinos (which would make the leptonic width actually a LNC mode) in the event is far from trivial too: One would need to establish either that the escaping particle is massive (SM neutrinos are “massless” for the LHC) or demonstrate (for example, by studying the energy distributions of the charged leptons) that only a single particle has escaped detection (and not two, as would be necessary to compensate the lepton number of the two charged leptons). In summary, it seems possible, in principle, to show experimentally that the LHC has found LNV and thus traces of the origin of neutrino mass. However, in practice to make all necessary measurements requires that the model is realized in nature within some particularly favourable part of parameter space.

To summarize, we have studied the dark matter and LHC phenomenology of a neutrino mass model, which contains a doubly charged scalar. Long-lived and quasi-stable particle searches at the LHC might discover such a state in the future and thus, distinguish this model from its famous scotogenic cousin. As we have briefly discussed here, these LHC

searches are actually sensitive to a large fraction of all 1-loop neutrino mass models in this “dark matter” class.

Acknowledgements

G.C. thanks Gabriel Torrealba for his help with python and Andre Lessa for useful comments. M.H. is supported by the Spanish grants PID2020-113775GB-I00 (AEI/10.13039/501100011033), CIPROM/2021/054 (Generalitat Valenciana) and the MultiDark network, RED2022-134411-T. G.C. acknowledges support from ANID FONDECYT grant No. 11220237. J.C.H. acknowledges support from ANID FONDECYT grant No.1241685. T.B.M acknowledges support from ANID FONDECYT grant No. 3220454. G.C., J.C.H. and T.B.M. also acknowledge support from ANID - Millennium Science Initiative Program ICN2019_044. C.A. is supported by ANID-Chile FONDECYT grant No. 1231248 and ANID-Chile PIA/APOYO AFB230003.

References

- [1] Z.-j. Tao, *Radiative seesaw mechanism at weak scale*, *Phys. Rev. D* **54** (1996) 5693 [[hep-ph/9603309](#)].
- [2] E. Ma, *Verifiable radiative seesaw mechanism of neutrino mass and dark matter*, *Phys. Rev. D* **73** (2006) 077301 [[hep-ph/0601225](#)].
- [3] L. Lopez Honorez, E. Nezri, J.F. Oliver and M.H.G. Tytgat, *The Inert Doublet Model: An Archetype for Dark Matter*, *JCAP* **02** (2007) 028 [[hep-ph/0612275](#)].
- [4] A. Vicente and C.E. Yaguna, *Probing the scotogenic model with lepton flavor violating processes*, *JHEP* **02** (2015) 144 [[1412.2545](#)].
- [5] E. Molinaro, C.E. Yaguna and O. Zapata, *FIMP realization of the scotogenic model*, *JCAP* **07** (2014) 015 [[1405.1259](#)].
- [6] A.G. Hessler, A. Ibarra, E. Molinaro and S. Vogl, *Probing the scotogenic FIMP at the LHC*, *JHEP* **01** (2017) 100 [[1611.09540](#)].
- [7] S. Baumholzer, V. Brdar, P. Schwaller and A. Segner, *Shining Light on the Scotogenic Model: Interplay of Colliders and Cosmology*, *JHEP* **09** (2020) 136 [[1912.08215](#)].
- [8] T. de Boer, R. Busse, A. Kappes, M. Klasen and S. Zeinstra, *Indirect detection constraints on the scotogenic dark matter model*, *JCAP* **08** (2021) 038 [[2105.04899](#)].
- [9] L. Eisenberger, T. Siebert, K. Mannheim and W. Porod, *MHz to TeV expectations from scotogenic WIMP dark matter*, [2310.10421](#).
- [10] I.M. Ávila, V. De Romeri, L. Duarte and J.W.F. Valle, *Phenomenology of scotogenic scalar dark matter*, *Eur. Phys. J. C* **80** (2020) 908 [[1910.08422](#)].
- [11] I.M. Ávila, G. Cottin and M.A. Díaz, *Revisiting the scotogenic model with scalar dark matter*, *J. Phys. G* **49** (2022) 065001 [[2108.05103](#)].
- [12] J. Liu, Z.-L. Han, Y. Jin and H. Li, *Unraveling the Scotogenic model at muon collider*, *JHEP* **12** (2022) 057 [[2207.07382](#)].
- [13] A. Beniwal, J. Herrero-García, N. Leerdam, M. White and A.G. Williams, *The ScotoSinglet Model: a scalar singlet extension of the Scotogenic Model*, *JHEP* **21** (2020) 136 [[2010.05937](#)].
- [14] M. Hirsch, R.A. Lineros, S. Morisi, J. Palacio, N. Rojas and J.W.F. Valle, *WIMP dark matter as radiative neutrino mass messenger*, *JHEP* **10** (2013) 149 [[1307.8134](#)].
- [15] C. Hagedorn, J. Herrero-García, E. Molinaro and M.A. Schmidt, *Phenomenology of the Generalised Scotogenic Model with Fermionic Dark Matter*, *JHEP* **11** (2018) 103 [[1804.04117](#)].
- [16] P. Escribano, M. Reig and A. Vicente, *Generalizing the Scotogenic model*, *JHEP* **07** (2020) 097 [[2004.05172](#)].
- [17] S. Kanemura, O. Seto and T. Shimomura, *Masses of dark matter and neutrino from TeV scale spontaneous $U(1)_{B-L}$ breaking*, *Phys. Rev. D* **84** (2011) 016004 [[1101.5713](#)].
- [18] D. Portillo-Sánchez, P. Escribano and A. Vicente, *Ultraviolet extensions of the Scotogenic model*, *JHEP* **08** (2023) 023 [[2301.05249](#)].

- [19] V. De Romeri, J. Nava, M. Puerta and A. Vicente, *Dark matter in the scotogenic model with spontaneous lepton number violation*, *Phys. Rev. D* **107** (2023) 095019 [2210.07706].
- [20] R.A. Lineros and M. Pierre, *Dark matter candidates in a type-II radiative neutrino mass model*, *JHEP* **21** (2020) 072 [2011.08195].
- [21] Y. Farzan, S. Pascoli and M.A. Schmidt, *AMEND: A model explaining neutrino masses and dark matter testable at the LHC and MEG*, *JHEP* **10** (2010) 111 [1005.5323].
- [22] F. Bonnet, M. Hirsch, T. Ota and W. Winter, *Systematic study of the $d=5$ Weinberg operator at one-loop order*, *JHEP* **07** (2012) 153 [1204.5862].
- [23] C. Arbeláez, R. Cepedello, J.C. Helo, M. Hirsch and S. Kovalenko, *How many 1-loop neutrino mass models are there?*, *JHEP* **08** (2022) 023 [2205.13063].
- [24] S. Bottaro, D. Buttazzo, M. Costa, R. Franceschini, P. Panci, D. Redigolo et al., *Closing the window on WIMP Dark Matter*, *Eur. Phys. J. C* **82** (2022) 31 [2107.09688].
- [25] S. Bottaro, D. Buttazzo, M. Costa, R. Franceschini, P. Panci, D. Redigolo et al., *The last Complex WIMPs standing*, 2205.04486.
- [26] PLANCK collaboration, *Planck 2018 results. VI. Cosmological parameters*, *Astron. Astrophys.* **641** (2020) A6 [1807.06209].
- [27] LZ collaboration, *First Dark Matter Search Results from the LUX-ZEPLIN (LZ) Experiment*, *Phys. Rev. Lett.* **131** (2023) 041002 [2207.03764].
- [28] XENON collaboration, *First Dark Matter Search with Nuclear Recoils from the XENONnT Experiment*, *Phys. Rev. Lett.* **131** (2023) 041003 [2303.14729].
- [29] P.F. de Salas, D.V. Forero, S. Gariazzo, P. Martínez-Miravé, O. Mena, C.A. Ternes et al., *2020 global reassessment of the neutrino oscillation picture*, *JHEP* **02** (2021) 071 [2006.11237].
- [30] T. Toma and A. Vicente, *Lepton Flavor Violation in the Scotogenic Model*, *JHEP* **01** (2014) 160 [1312.2840].
- [31] C.-L. Shan, *Determining the Mass of Dark Matter Particles with Direct Detection Experiments*, *New J. Phys.* **11** (2009) 105013 [0903.4320].
- [32] S.D. McDermott, H.-B. Yu and K.M. Zurek, *The Dark Matter Inverse Problem: Extracting Particle Physics from Scattering Events*, *Phys. Rev. D* **85** (2012) 123507 [1110.4281].
- [33] R.M. Fonseca, *The Sym2Int program: going from symmetries to interactions*, *J. Phys. Conf. Ser.* **873** (2017) 012045 [1703.05221].
- [34] M. Cirelli, N. Fornengo and A. Strumia, *Minimal dark matter*, *Nucl. Phys. B* **753** (2006) 178 [hep-ph/0512090].
- [35] I. Cordero-Carrión, M. Hirsch and A. Vicente, *General parametrization of Majorana neutrino mass models*, *Phys. Rev. D* **101** (2020) 075032 [1912.08858].
- [36] F. Staub, *SARAH 4 : A tool for (not only SUSY) model builders*, *Comput. Phys. Commun.* **185** (2014) 1773 [1309.7223].
- [37] F. Staub, *SARAH 3.2: Dirac Gauginos, UFO output, and more*, *Comput. Phys. Commun.* **184** (2013) 1792 [1207.0906].

- [38] W. Porod, *SPheno, a program for calculating supersymmetric spectra, SUSY particle decays and SUSY particle production at e^+e^- colliders*, *Comput. Phys. Commun.* **153** (2003) 275 [[hep-ph/0301101](#)].
- [39] W. Porod and F. Staub, *SPheno 3.1: Extensions including flavour, CP-phases and models beyond the MSSM*, *Comput. Phys. Commun.* **183** (2012) 2458 [[1104.1573](#)].
- [40] G. Belanger, F. Boudjema, A. Pukhov and A. Semenov, *micrOMEGAs.3: A program for calculating dark matter observables*, *Comput. Phys. Commun.* **185** (2014) 960 [[1305.0237](#)].
- [41] J. Alwall, P. Demin, S. de Visscher, R. Frederix, M. Herquet, F. Maltoni et al., *MadGraph/MadEvent v4: The New Web Generation*, *JHEP* **09** (2007) 028 [[0706.2334](#)].
- [42] J. Alwall, M. Herquet, F. Maltoni, O. Mattelaer and T. Stelzer, *MadGraph 5 : Going Beyond*, *JHEP* **06** (2011) 128 [[1106.0522](#)].
- [43] G. Arcadi, A. Djouadi and M. Raidal, *Dark Matter through the Higgs portal*, *Phys. Rept.* **842** (2020) 1 [[1903.03616](#)].
- [44] J.M. Cline, K. Kainulainen, P. Scott and C. Weniger, *Update on scalar singlet dark matter*, *Phys. Rev. D* **88** (2013) 055025 [[1306.4710](#)].
- [45] S. Bhattacharya, P. Ghosh, A.K. Saha and A. Sil, *Two component dark matter with inert Higgs doublet: neutrino mass, high scale validity and collider searches*, *JHEP* **03** (2020) 090 [[1905.12583](#)].
- [46] A. Dutta Banik, R. Roshan and A. Sil, *Two component singlet-triplet scalar dark matter and electroweak vacuum stability*, *Phys. Rev. D* **103** (2021) 075001 [[2009.01262](#)].
- [47] K. Griest and D. Seckel, *Three exceptions in the calculation of relic abundances*, *Phys. Rev. D* **43** (1991) 3191.
- [48] M. Schumann, L. Baudis, L. Bütikofer, A. Kish and M. Selvi, *Dark matter sensitivity of multi-ton liquid xenon detectors*, *JCAP* **10** (2015) 016 [[1506.08309](#)].
- [49] ATLAS collaboration, *Search for massive, long-lived particles using multitrack displaced vertices or displaced lepton pairs in pp collisions at $\sqrt{s} = 8$ TeV with the ATLAS detector*, *Phys. Rev. D* **92** (2015) 072004 [[1504.05162](#)].
- [50] CMS collaboration, *Search for displaced leptons in the e -mu channel*, .
- [51] ATLAS collaboration, *Search for Displaced Leptons in $\sqrt{s} = 13$ TeV pp Collisions with the ATLAS Detector*, *Phys. Rev. Lett.* **127** (2021) 051802 [[2011.07812](#)].
- [52] F. Blekman, N. Desai, A. Filimonova, A.R. Sahasransu and S. Westhoff, *Soft displaced leptons at the LHC*, *JHEP* **11** (2020) 112 [[2007.03708](#)].
- [53] ATLAS collaboration, *Search for displaced vertices of oppositely charged leptons from decays of long-lived particles in pp collisions at $\sqrt{s} = 13$ TeV with the ATLAS detector*, *Phys. Lett. B* **801** (2020) 135114 [[1907.10037](#)].
- [54] ATLAS collaboration, *Search for long-lived, massive particles in events with displaced vertices and missing transverse momentum in $\sqrt{s} = 13$ TeV pp collisions with the ATLAS detector*, *Phys. Rev. D* **97** (2018) 052012 [[1710.04901](#)].
- [55] CMS collaboration, *Search for long-lived particles using displaced vertices and missing transverse momentum in proton-proton collisions at $\sqrt{s} = 13$ TeV*, **2402.15804**.

- [56] ATLAS collaboration, *Search for heavy long-lived multi-charged particles in the full LHC Run 2 pp collision data at $s=13$ TeV using the ATLAS detector*, *Phys. Lett. B* **847** (2023) 138316 [[2303.13613](#)].
- [57] C.A. R, G. Cottin, J.C. Helo and M. Hirsch, *Long-lived charged particles and multi-lepton signatures from neutrino mass models*, *Phys. Rev. D* **101** (2020) 095033 [[2003.11494](#)].
- [58] M. Hirsch, R. Maselek and K. Sakurai, *Detecting long-lived multi-charged particles in neutrino mass models with MoEDAL*, *Eur. Phys. J. C* **81** (2021) 697 [[2103.05644](#)].
- [59] J. Alwall, R. Frederix, S. Frixione, V. Hirschi, F. Maltoni, O. Mattelaer et al., *The automated computation of tree-level and next-to-leading order differential cross sections, and their matching to parton shower simulations*, *JHEP* **07** (2014) 079 [[1405.0301](#)].
- [60] A. Buckley, J. Ferrando, S. Lloyd, K. Nordström, B. Page, M. Rüfenacht et al., *LHAPDF6: parton density access in the LHC precision era*, *Eur. Phys. J. C* **75** (2015) 132 [[1412.7420](#)].
- [61] T. Sjöstrand, S. Ask, J.R. Christiansen, R. Corke, N. Desai, P. Ilten et al., *An introduction to PYTHIA 8.2*, *Comput. Phys. Commun.* **191** (2015) 159 [[1410.3012](#)].
- [62] M. Cacciari, G.P. Salam and G. Soyez, *FastJet User Manual*, *Eur. Phys. J. C* **72** (2012) 1896 [[1111.6097](#)].
- [63] G. Cottin, J.C. Helo and M. Hirsch, *Searches for light sterile neutrinos with multitrack displaced vertices*, *Phys. Rev. D* **97** (2018) 055025 [[1801.02734](#)].
- [64] G. Brooijmans et al., *Les Houches 2017: Physics at TeV Colliders New Physics Working Group Report*, in *10th Les Houches Workshop on Physics at TeV Colliders*, 3, 2018 [[1803.10379](#)].
- [65] ATLAS collaboration, *Search for long-lived charginos based on a disappearing-track signature using 136 fb^{-1} of pp collisions at $\sqrt{s} = 13$ TeV with the ATLAS detector*, *Eur. Phys. J. C* **82** (2022) 606 [[2201.02472](#)].
- [66] CMS collaboration, *Search for supersymmetry in final states with disappearing tracks in proton-proton collisions at $\sqrt{s} = 13$ TeV*, [2309.16823](#).
- [67] G. Alguero, J. Heisig, C.K. Khosa, S. Kraml, S. Kulkarni, A. Lessa et al., *Constraining new physics with SModelS version 2*, *JHEP* **08** (2022) 068 [[2112.00769](#)].
- [68] A. Collaboration, “https://atlas.web.cern.ch/Atlas/GROUPS/PHYSICS/PAPERS/SUSY-2016-08/hepdata_info.pdf.”.
- [69] CMS collaboration, *Search for long-lived charged particles in proton-proton collisions at $\sqrt{s} = 13$ TeV*, *Phys. Rev. D* **94** (2016) 112004 [[1609.08382](#)].
- [70] G. Cottin, J.C. Helo, M. Hirsch, C. Peña, C. Wang and S. Xie, *Long-lived heavy neutral leptons with a displaced shower signature at CMS*, *JHEP* **02** (2023) 011 [[2210.17446](#)].